UNIVERSITY OF DELAWARE

INSTITUTE OF
ENERGY CONVERSION

451 Wyoming Road
Newark, DE 19716-3820
Ph: 302/831-6200
Fax: 302/831-6226
www.udel.edu/iec

UNITED STATES DEPARTMENT OF ENERGY
UNIVERSITY CENTER OF EXCELLENCE
FOR PHOTOVOLTAIC RESEARCH AND EDUCATION

August 27, 2008

Bolko von Roedern
National Renewable Energy Laboratory
1617 Cole Boulevard
Golden, CO 80401

Re: NREL Subcontract #ADJ-1-30630-12
D.5.35

Dear Bolko,

This report covers research conducted at the Institute of Energy Conversion (IEC) for the period of April 1, 2008 to April 30, 2008, under the subject subcontract. The report presents results obtained for research under Task 1, CdTe-based solar cells. During this period, effort was focused on two sub-tasks: 1.1) fabrication of devices with thin CdTe absorber layers, and 1.2) development of mechanically flexible CdTe cells by deposition onto a temporary support followed by transfer to a flexible polymer substrate.

1.1 Thin CdTe Absorbers

The primary objective of this sub-task is to specify deposition and vapor $CdCl_2$ post-deposition treatment conditions needed for high throughput processing (1-2 min per plate) of polycrystalline thin film CdS/CdTe solar cells with sub-micron CdTe. This requires characterization of the grain size distribution obtained during CdTe film growth which affects the delivery of $CdCl_2$ and O_2 to the CdTe film and influences CdTe-CdS inter diffusion. VT deposition allows great flexibility in CdTe film growth, with static deposition rates up to ~100 μm/min. However, cells with thin absorbers and deposited at high translation speeds do not require such high growth rates to obtain high throughput, so lower source temperatures can be employed for CdTe film growth.

In polycrystalline CdTe films, the chemical reactivity obtained during treatment is enhanced by the presence of grain boundaries, which allow $CdCl_2$ and O_2 to penetrate the film, reach the CdS-CdTe interface and react along grain surfaces. The fractional grain boundary volume increases as grain size decreases. For a tessellated hexagonal array of uniform grains with 1:1 aspect ratio, a decrease in film thickness produces a decrease in lateral grain size. For a reduction from 10 μm to 0.5 μm, the contact perimeter increases from 60 μm to 140 μm and ratio of grain boundary to grain volume increases from 0.004 to 0.7. The optimization of superstrate

CdTe/CdS solar cells is accomplished by a combination of surface reaction and diffusion. The diffusion of defects from CdTe grain surfaces into grain interiors is driven by the concentration gradient on the CdTe surface and along grain walls. The time needed to diffuse defects into grain interiors relies on the diffusivity of cadmium vacancies (V_{Cd}). At the same time, the thermodynamic driving force for CdS-CdTe intermixing drives interface diffusion, limited by Cd self-diffusion through the CdTe lattice. By specifying the processing time, the problem is to find the bulk diffusion coefficient (D_B) needed to accommodate the particular grain size distribution and specified processing time,

$$D_B = \frac{r^2}{\tau} \tag{1}$$

where r is half the grain size and τ is the characteristic time. For the example of films with 10 μm and 0.5 μm grain size, the characteristic diffusion time at constant temperature is reduced by 400X. Although the bulk diffusion coefficients for V_{Cd} are unknown, the optimization process for solar cell performance controls Cd self-diffusion; likely the slowest process and is therefore a reasonable limit. Also, the consumption of CdS needs to be considered as the grain size or temperature is changed. Therefore, processing temperatures follow from the bulk diffusion process for Cd self diffusion and the grain boundary diffusion process for CdS in CdTe (D_{GB}):

$$D_B = 2.4\text{x}10^7 e^{-\left(\frac{2.8}{kT}\right)} \text{ cm}^2/\text{s} \tag{2}$$

$$D_{GB} = 3.4\text{x}10^6 e^{-\left(\frac{2.0}{kT}\right)} \text{ cm}^2/\text{s} \tag{3}$$

for treatment in 9 mTorr $CdCl_2$ and 150 mTorr O_2. D_{GB} depends on $CdCl_2$ partial pressure (P_{sat}) over the range 1 to 100 mTorr:

$$D_{GB} = 9.0\text{x}10^4 P_{sat}^{2.73} e^{-\left(\frac{2.0}{kT}\right)} \text{ cm}^2/\text{s} \tag{4}$$

Only the grain boundary diffusion, via surface reactions is sensitive to both $CdCl_2$ and O_2 concentration. For CdTe films deposited by VT at 550°C processing with vapor $CdCl_2$ treatment in the 1-2 min time frame is considered. The properties of solar cells fabricated with these films are reported and discussed with respect to the absorber thickness.

The vapor treatment method allows $CdCl_2$ concentration to be independently controlled from the CdTe/CdS sample temperature. As found with conventional $CdCl_2$ treatment, the vapor $CdCl_2$ treatment promotes diffusion of CdS into CdTe films. For VT CdTe films deposited at 550-600°C in N_2/O_2 ambient, no grain growth is detected following the $CdCl_2$ treatment, indicating that as-deposited VT CdTe films are in a low energy state compared to PVD films of the same thickness. 3D modeling of CdS diffusion into CdTe using measured grain size distributions shown in the previous report (for January 2008 of this contract) and previously determined bulk and grain boundary diffusion coefficients and activation energies (Equations 2-4 above), the temperature-time conditions were determined to produce similar diffusion profiles but at markedly reduced processing time.

Fig. 1 shows calculated $CdTe_{1-x}S_x$ depth profile plots (c/co versus depth) for films from 5 to 0.5 μm thickness using the measured grain size distributions of VT CdTe films with the corresponding thickness, calculated for baseline vapor $CdCl_2$ treatment under the following

conditions: isothermal vapor $CdCl_2$ treatment at 420°C for 20 minutes (420°C/20 min) at 1 atm, with 150 mTorr O_2 partial pressure. In this case, the $CdCl_2$ partial pressure is 9 mTorr and the bulk and grain boundary diffusion coefficients used were: $D_B = 1.2 \times 10^{-13}$ cm^2/s and $D_{GB} = 1.1 \times 10^{-8}$ cm^2/s, respectively. In the figure, the bulk and grain boundary contributions are apparent by the steep and flat regions, respectively. For films <3 µm, thick, the bulk contribution is more apparent due to decreasing lateral dimension compared to the bulk characteristic diffision distance. Integration of the curves with the $CdTe_{1-x}S_x$ solubility limit at 420°C (x = 0.06) allows the equivalent CdS film consumed to be estimated and is indicated on the right side of the plot. For the typical baseline film (5 µm) treated at 420ºC for 20 minutes, the least alloy formation is obtained, with an equivalent CdS film thickness consumed of only 20 nm. This corresponds extremely well to the measured final CdS thickness after cell fabrication and physical removal of the $CdTe_{1-x}S_x$ absorber layer. For the thinner CdTe films, the equivalent CdS thickness consumed is slightly greater and shows that uniform $CdTe_{1-x}S_x$ alloy production is expected for films > 0.5 µm thick.

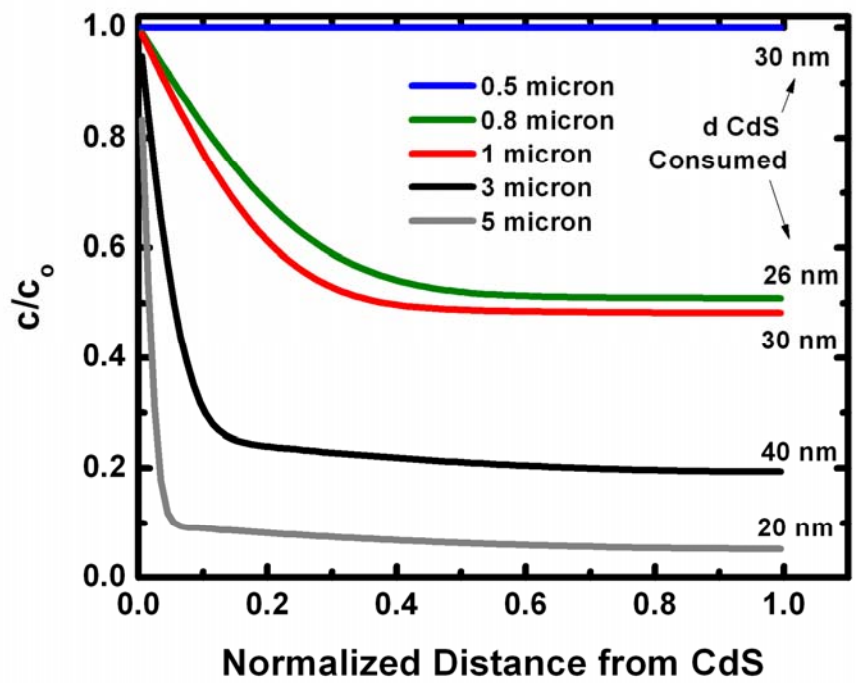

Figure 1. Calculated S concentration (c/co) versus normalized distance from CdS-CdTe interface for CdS/CdTe couples with different CdTe thickness. The calculation used the measured grain size distribution and diffusion coefficients corresponding to baseline vapor $CdCl_2$ treatment at 420°C for 20 minutes.

Reduced vapor $CdCl_2$ treatment time is facilitated by increasing reaction temperature without changing other parameters. For example, with a 5 µm CdTe film; nominally similar CdS consumption is obtained for temperature/time treatments of 420ºC/20 min, 480ºC/2 min, and 495ºC/1 min in 9 mTorr $CdCl_2$ and 150 Torr O_2. For the shorter cases, at 480ºC for 2 minutes and 495ºC for 1 minute, the equivalent CdS thicknesses consumed is 2X higher, ~40 nm. An extreme case, at 480ºC for 20 minutes, shows consumption of 100 nm of CdS, which would eliminate the CdS layer in these 5 µm thick devices. Extending these calculations to thinner

films using Equations 2-4 to find D_B and D_{GB} enables benchmark treatment temperatures to be specified for 2 min treatments (Table I).

Table I. Temperature benchmarks for vapor $CdCl_2$ treatment of CdS/CdTe with different CdTe thickness.

CdTe Thk (μm)	T Reaction (°C)	T $CdCl_2$ (°C)
5	480	420
3	475	420
1	470	415
0.8	465	415
0.5	460	410
0.3	460	410

The AM1.5 performance of baseline (5 μm thick CdTe) VT CdTe cells fabricated with vapor $CdCl_2$ treatment at 480ºC with $CdCl_2$ time from 1 to 4 min is shown in Table II. The quantum efficiency (QE) at $\lambda = 400$ nm provides a quantitative measure of the final CdS film thickness. In the table, the final CdS film thickness decreases progressively with increasing treatment time over the treatment time range. Given that the starting CdS thickness was 90 nm, the quantity of CdS consumed is comparable to that predicted by the diffusion model above for 5 μm thick films. The cell performance data shows that optimal V_{OC} is obtained for 2-4 min treatment while optimal FF is obtained for 1-2 min treatment. Although the CdS thickness was slightly affected by the treatment time, the J_{SC} was not significantly different.

Table II. Best-cell J-V results for VT cells with baseline 5 μm CdTe deposited and vapor $CdCl_2$ treatment at 480ºC with different $CdCl_2$ time.

$CdCl_2$ HT (min)	V_{OC} (mV)	J_{SC} (mA/ cm^2)	FF (%)	η (%)	QE @ 400nm (%)	Final dCdS (nm)
1	783	23.6	66.6	12.3	40	60
2	796	24.3	69.4	13.4	42	58
2	813	23.6	66.2	12.7	44	55
2.5	800	23.3	65.1	12.2	44	55
4	819	24.3	64.6	12.9	50	35

The treatment conditions of Table I were adopted for the fabrication of solar cells with thinner VT CdTe absorber layers. The effect of the BDH etch process was evaluated on samples with different CdTe absorber thickness and 2 min treatment time. A small sample set was sufficient to indicate a dramatic drop in both V_{OC} and FF for cells with absorber thickness <2 μm (Fig 2). The degree of shunting increased as CdTe thickness was reduced, and many cells were shorted completely. The shunt conductance of baseline cells is typically 1 mS-cm^2 and increased to >20 mS-cm^2 for 1 μm CdTe.

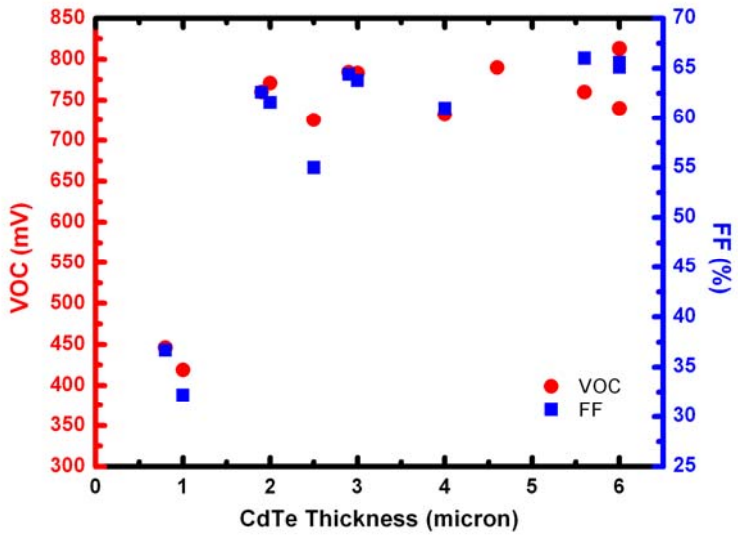

Figure 2. V_{OC} (red circles, left axis) and FF (blue squares, right axis) of CdS/CdTe cells processed with 2 min $CdCl_2$ treatment and BDH etch.

A milder surface etch using bromine-methanol (BrMeOH) yielded demonstrable improvement in device yield and tolerance to thinner absorber layers. Fig. 3 shows V_{OC} and FF of cells obtained with thin VT CdTe absorbers using the $CdCl_2$ protocols of Table III with 2 minute treatments and BrMeOH etch. Baseline V_{OC} is retained down to an absorber thickness of 1.5 µm and follows a monotonic falloff thereafter. The best FF obtained with the BrMeOH etch is comparable to that achieved with the BDH etch but drops progressively with reduced CdTe thickness. However, the FF on cells using the BrMeOH etch are not dominated by shunt conductance. The area yield of cells processed with vapor treatment and mild BrMeOH approaches 100%, which verifies the low pinhole density and demonstrates the benign nature of this back contact process.

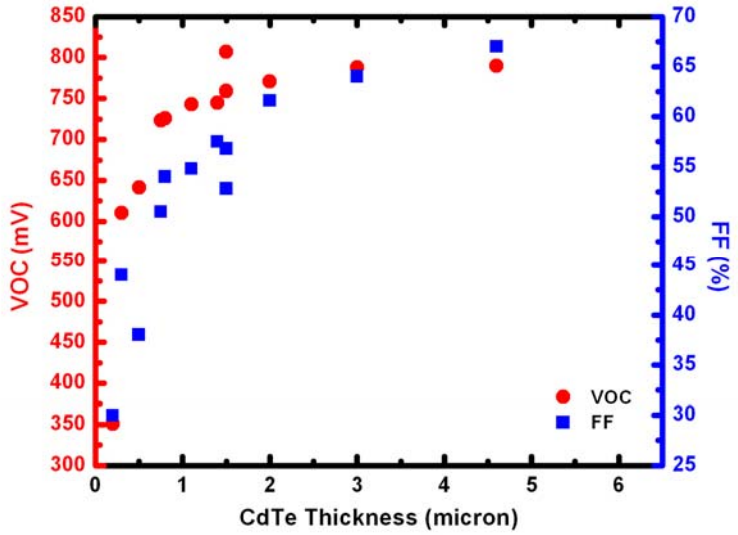

Figure 3. V_{OC} (red circles, left axis) and FF (blue squares, right axis) of CdS/CdTe cells processed with 2 min $CdCl_2$ treatment and BrMeOH etch.

The best cell results obtained for VT cells with thin CdTe absorber layers using 2 min vapor $CdCl_2$ treatment at 480°C and BrMeOH etching are listed in Table III. The V_{OC} and FF decrease with reduced CdTe thickness, while J_{SC} remains relatively constant, dropping by ~1 mA/cm^2 for the cell with 0.8 µm thick CdTe.

Table III. Best-cell J-V results for VT cells with thin CdTe absorber layers using vapor $CdCl_2$ treatment at 480ºC with 2 minute $CdCl_2$ time and etched with BrMeOH.

CdTe Thickness (µm)	V_{OC} (mV)	J_{SC} (mA/cm^2)	FF (%)	η (%)
3.0	788	23.1	64.0	11.8
1.5	807	23.8	56.8	10.9
1.0	743	23.4	54.8	9.5
0.8	723	22.5	50.5	8.2

Some device sets, however, exhibit lower photocurrent than expected, based on the CdTe absorption data presented in the previous report (for January 2008 of this contract). The raw and normalized quantum efficiency (QE) of cells with thin CdTe are compared to a baseline cell (5 µm) in Figs. 4 and 5, respectively. The normalized data shows a shift in peak response towards the blue and the expected loss in the red. The raw data shows a 2X panchromatic loss not accounted for by decreased absorption, and QE measurements at reverse bias did not significantly improve collection. Thus, while the photo-response *profile* is attributable to optical absorption, the magnitude is related to photo-carrier recombination. This behavior is correlated with the TEC15 glass batch, and more analysis is required to relate the behavior to glass impurities, effectiveness of the HRT layer as a diffusion barrier, and device processing.

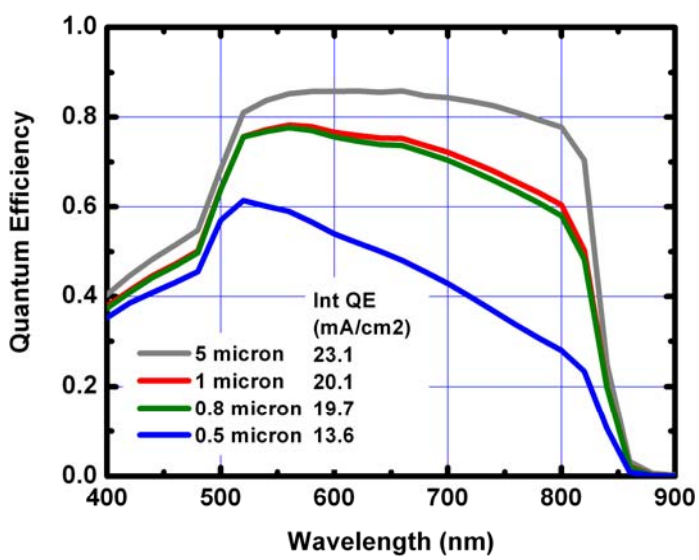

Figure 4. Raw QE (0V, light) of CdS/CdTe cells with baseline (top) and thin CdTe absorbers processed with 2 min $CdCl_2$ treatment.

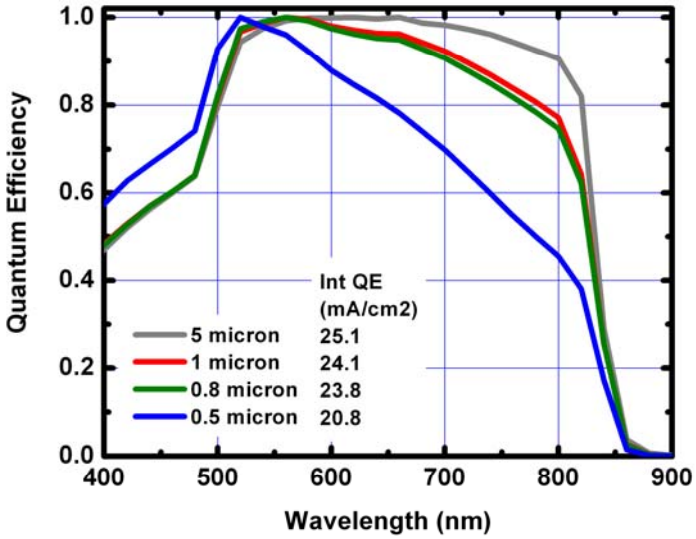

Figure 5. Normalized QE of CdS/CdTe cells with baseline (top) and thin CdTe absorbers of Figure 4.

Past x-ray diffraction and photoemission spectroscopic analyses of the surface of vapor $CdCl_2$ treated CdTe films showed the total oxide thickness to be <5 nm, suggesting the possibility of eliminating the etch step altogether for samples prepared with brief vapor $CdCl_2$ treatments. Cells with 3-5 µm CdTe fabricated with short vapor $CdCl_2$ treatment and no etch step yielded 12% conversion efficiencies.

1.2 Flexible CdTe Solar Cell

Additional device structures were made using PVD CdS and VT CdTe films on ITO-coated Al foil superstrates. Cell transfer to flexible Upilex substrates was carried out using the same conductive Ag epoxy as reported in the previous report (for January 2008 of this contract). The temperature and strength of the NaOH bath needed to remove the Al was varied in an attempt to overcome the cracking phenomenon obtained for the conditions previously employed. The etch rate for Al foil was determined by measuring the time to completely etch 1 x 1 cm pieces in aqueous NaOH solution at different concentration and temperature. The etch rate results are listed in Table IV.

Table IV. Al foil etch rate for different NaOH solution concentration and temperature.

Temp (ºC) ± 1º C	**$NaOH:H_2O$ Strength (Molar)**		
	0.1	**0.5**	**1**
	Etch rate (µm/min)		
30	0.29	0.73	0.85
40	0.45	1.50	1.86
50	0.74	1.85	2.48
60	1.26	3.79	4.97

Experiments with actual device structures were carried out at two extreme points in Table IV: 0.1 Mol/30°C and 1 Mol/60°C. At 60°C, significant bubble formation at the edges caused undercutting of the device at the Ni/Ag epoxy interface, even after application of Kapton tape edge sealant. In addition, the Mo was damaged at the Mo/Upilex interface as a result of etching at regions of residual stress and oxidation (Mo grain surfaces), as a consequence of the Mo deposition conditions needed to deposit adherent Mo films on polyimide. At 30°C, the etch time was excessively long, and the entire structure was immersed in the bath for nearly an hour. In both cases, the transferred devices exhibit no detectable photoresponse. On-going effort is directed at evaluating alternative adhesives and mechanically robust and chemically inert back contact materials and configurations. The results will be presented in the Final report for the contract.

Best regards,

Robert W. Birkmire
Director